The Extension of the NIST BRDF Scale from 1100 nm to 2500 nm

Howard W. Yoon*, David W. Allen, George P. Eppeldauer, Benjamin K. Tsai
Optical Technology Division
National Institute of Standards and Technology,
Gaithersburg, MD, USA 20899

ABSTRACT

Measurements of bi-directional reflectance factor for diffuse reflectance from 1100 nm to 2500 nm using extended-range indium gallium arsenide (exInGaAs) detectors in the NIST Spectral Tri-function Automated Reference Reflectometer (STARR) facility are described. The determination of bi-directional reflectance factor with low uncertainties requires the exInGaAs radiometer to be characterized for low-noise performance, linearity and spatial uniformity. The instrument characterizations will be used to establish a total uncertainty budget for the reflectance factor. To independently check the bi-directional reflectance factors, measurements also were made in a separate facility in which the reflectance factor is determined using calibrated spectral irradiance and radiance standards. The total combined uncertainties for the diffuse reflectances range from < 1 % at 1100 nm to 2.5 % at 2500 nm. At NIST, these measurement capabilities will evolve into a calibration service for diffuse spectral reflectance in this wavelength region.

Keywords: bi-directional reflectance factors, infrared, pressed PTFE, absolute reflectance

1. INTRODUCTION

Due to the increasing needs to monitor the Earth's accelerating climate change, remote sensing instruments are used to measure the spectral radiances in the Earth's reflected solar wavelengths from 250 nm to 2500 nm. Since information about the moisture content of the vegetation, among other scientific data products, can be obtained from measurements in the short-wave infrared region, instruments such as the Landsat 7 and the Operational Land Imager specifically have spectral filters at near 1.6 μm and at 2.2 μm[1]. These instruments are typically calibrated for spectral radiance responsivity using integrating sphere sources (ISS) traceable to NIST. Since the sensors typically have large field-of-views, ISS's with large openings are needed for their calibrations. These large ISS's are not easily transported and thus transfer calibrations from smaller NIST calibrated integrating spheres are used with potentially increased uncertainties from the possible drift of the integrating sphere radiances. Calibrations of remote sensing instruments for spectral radiance responsivity can also be performed using spectral irradiance standards and reflectance standards[2]. These reflectance standards can also be used for in-orbit monitoring of the spectral radiance responsivities of the satellite sensors using the sun as a source of spectral irradiance. Although these methods are well established in the visible wavelength region,[3] the extension to the short-wave infrared region requires the determination of bi-directional reflectance factors with low uncertainties.

One of the main impediments to the realization of the bi-directional diffuse reflectance scale to 2500 nm is the need to measure the extremely low reflected spectral signal with low uncertainties. The difficulties arise since a perfectly lambertian diffuser or nearly perfect diffuser such as pressed polytetrafluoroethylene (PTFE) or Spectralon# will direct the incident radiation into the 2π hemisphere such that only a small portion of the incident radiation can be collected in the determination of the reflectance factor. These difficulties are compounded by the fact that detectors which operated in the wavelength region from 1100 nm to 2500 nm with low noise, high shunt resistance, good spatial uniformity and linearity of responsivity have not been easily available, and calibration services for direct bi-directional reflectance factors are thus subsequently limited to < 1700 nm[4,5]. In the past, due to the absence of bi-directional reflectance factor measurements beyond 1700 nm, a constant ratio between the directional-hemispherical reflectance factor and the bi-directional reflectance factor from 250 nm to 1700 nm was used to extrapolate the bi-directional reflectance factor to 2500 nm.

*hyoon@nist.gov; phone 1 301 975-2482; fax 1 301 869-5700

In this work, we describe the use of a 4-stage thermo-electric cooled extended InGaAs (exInGaAs) detector with a single-element collection lens for the measurement of the bi-directional reflectance factor from 1100 nm to 2500 nm. The exInGaAs detector was constructed according to NIST designs with an integrated current-to-voltage preamplifier. The single-element lens was chosen to reduce the chromatic aberrations without greatly impacting the image quality. The radiometer was characterized for both gain linearity and frequency dependent gain. The reflectance measurements were made using the Spectral Tri-function Automated Reference Reflectometer (STARR)[6], the main NIST facility for reflectance measurements.

2. EXPERIMENTAL DESIGN

2.1 Measurement Problem

The bi-directional reflectance factors can be measured in different ways. The incident radiation can be quasi-monochromatic and generated using a lamp and a monochromator which is then measured using broad-band detection. Alternatively, broad-band sources can be used as sources of radiation with quasi-monochromatic detection using a monochromator in front of detectors. In the first case, as utilized in the STARR facility and illustrated in Fig. 1,

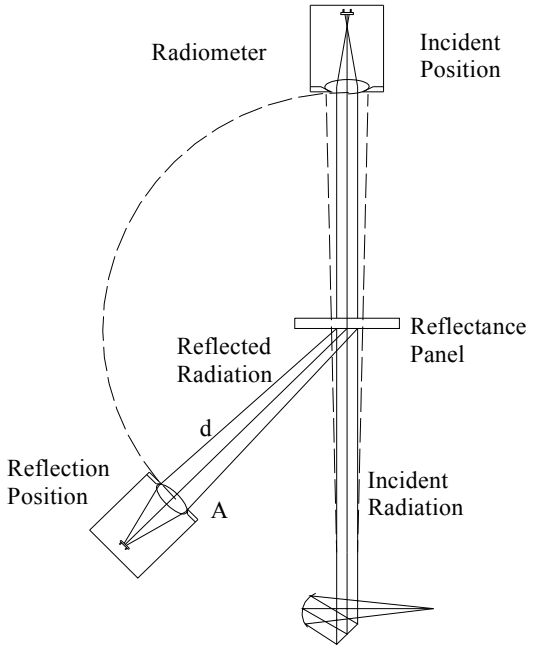

Fig. 1. Measurement setup in STARR using quasi-monochromatic incident radiation and broad-band detection for bi-directional reflectance factor determinations as described in Eq. 1. The dashed circle indicates the rotational movement of the radiometer. The dashed lines around the incident radiation illustrate the scatter from optical aberrations and scatter.

the reflectance factor is obtained from the reflected optical signal, S_r and the incident optical signal, S_i using

$$R = \pi \cdot \frac{S_r}{S_i} \cdot \frac{{d_S}^2}{A_r \cdot \cos \theta_r} \cdot \eta \ , \tag{1}$$

where d_S is the distance from the surface of the reflectance panel to the radiometer, A_r is the area of the entrance aperture of the radiometer, θ_r is the angle between the incident radiation and the optical axis of the radiometer and η is the gain factor between the two signals. If the same broad-band radiometer is used in the measurement of both the incident radiation and the reflected radiation, then the spectral responsivities need not be measured. The schematic shown in Fig. 1 is used at NIST and also at the Teknillinen korkeakoulu (TKK)[5].

It is also possible to measure the reflectance factor using a source of uniform radiance, L_i, with the reflectance factor,

$$R = \pi \cdot \frac{L_r}{L_i} \cdot \frac{{d_L}^2}{A_L \cdot \cos \theta_L} \cdot \eta \ , \tag{2}$$

where L_r is the radiance from the reflectance panel, d_L is the distance from the surface of the reflectance panel to the

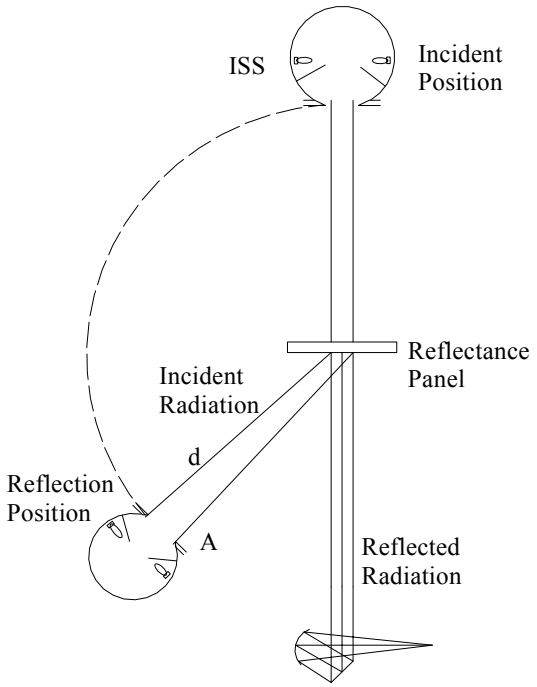

Fig. 2. Reflectance factor determinations using broad-band radiation from an integrating sphere source (ISS) and quasi-monochromatic detection as described in Eq. 2. The dotted circle indicates the rotational movement of the radiance source. The radiation path is reversed from the situation described in Fig. 1.

entrance aperture of the radiance source, A_L is the area of the exit aperture of the integrating sphere source, θ_L is the angle between the incident radiance and the reflected radiance, and η is the gain factor correction for the two radiances. In the situation described by Eq. 2, the broad-band radiometer shown in Fig. 1 would be replaced with a broad-band source and the optical path is reversed for the measurement of the reflected radiation using a spectroradiometer. The reflected radiances are measured using a spectrally dispersive instrument such as a monochromator or a spectrograph. Just as in the situation described in Eq. 1, if the same radiance source is used for the calibration and as the source of the incident radiation, then the spectral radiances of the source need not be determined. The schematic in Fig. 2 is used at Physikalisch-Technische Bundesanstalt (PTB)[4].

It is also possible to determine the radiance factor using two separate sources of spectral radiance and spectral irradiance. In Eq. 2, the incident spectral radiance, L_i, multiplied by the solid angle is the incident irradiance,

$$E_i = L_i \cdot \frac{A_L \cdot \cos \theta_L}{d_L^2} \, . \tag{3}$$

The reflectance factor is then simply,

$$R = \pi \cdot \frac{L_r}{E_i} \cdot \eta \,. \tag{4}$$

A source of calibrated spectral radiance must be utilized to determine the spectral radiance responsivity of the spectroradiometer, and a source of known spectral irradiance is used for the incident radiation. This approach is used in the NIST Irradiance Scale Realization Facility (ISRF)[7]. In this paper, we utilize techniques described in Eqs. 1 and 4. Although the equations are very similar, the three different approaches will have different component uncertainties due to the specific ways that the measurements are performed.

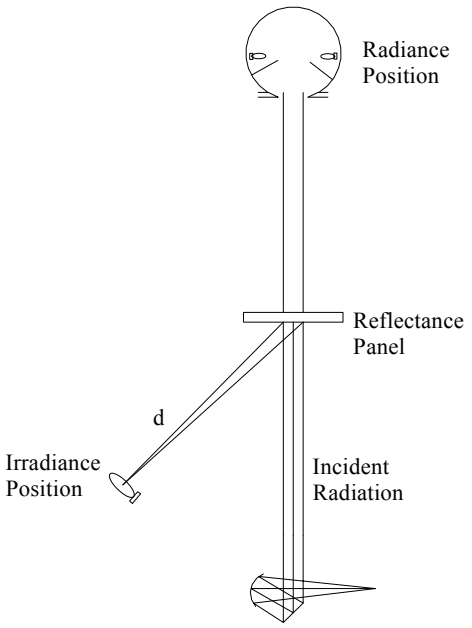

Fig. 3. Measurement setup in ISRF using quasi-monochromatic incident radiation and broad-band detection for bi-directional reflectance factor determinations. The integrating sphere source in the reflected position in Fig. 2 is replaced with a spectral irradiance standard lamp.

Without detailed comparisons between the three different realizations, it is difficult to generalize which measurement approach will result in the lowest uncertainties. Since the measurements are different, the uncertainty components will be different as well.

2.2 Choice of Detectors

A major barrier to the low uncertainty measurements of the diffuse reflectance in the infrared wavelength region is the low reflected signal. Briefly, the measurement apparatus of STARR, shown in Fig. 1, consists of a 100 W quartz-tungsten halogen (QTH) lamp focused into a single-grating monochromator with a 1 mm opening for a quasi-monochromatic radiation with a bandwidth of 14 nm. The output power from the monochromator is dependent upon the wavelength and is a convolved function of the spectral radiance of the QTH lamp, the imaged area of the lamp and the throughput of the spectroradiometer. For the system in STARR, at the spectral peak of 1000 nm the output power is about 1 uW. The need for low level measurements can be understood from the measurement geometry. The reflected signal can be estimated from the parameters of the measurement geometry and assumptions that the reflectance panel is lambertian or R=1. With these assumptions, the reflected optical power, S_r at the entrance aperture of the radiometer is

estimated to be about 1 x 10^{-4} smaller than the power in the incident radiation or < 100 pW. At the longest wavelengths, due to the reduced spectral radiance of the QTH lamp, the reflected optical power measured by the radiometer is estimated to be < 10 pW. Due to the low reflected signals as ratios of the incident signals, this measurement issue is evident at the different national measurement institutes as shown in Table 1.

Table 1. Calculated signals using the reported configurations in Refs. 4 and 5 for the bi-directional measurement setups at the respective national measurement institutes determined using Eqs. 1 and 2 for a perfect lambertian reflector.

	NIST	**PTB**	**TKK**
Distance (mm)	672.6	750	498.15
Aperture diameter (mm)	20.3	40	25
Angle	45	45	45
Incident signal	1	1	1
Calculated reflected signal	1.196E-04	3.736E-04	3.308E-04
Ratio (incident/reflected)	8359.0	2676.9	3023.3

In STARR, the output radiation from the monochromator is collimated using an off-axis parabolic mirror to a beam diameter of 17 mm. In the measurement of the incident beam, the radiation in the 17 mm diameter beam is directed into the larger 22 mm diameter aperture stop of the infrared radiometer as shown in Fig 4. In the measurement of the reflected beam, the entrance aperture of the radiometer is placed at a distance of 672.6 mm from the center of the 17 mm collimated beam incident on the reflectance panel. The incident radiation is diffusely scattered and acts as the object for the imaging radiometer.

It is difficult to measure these low signals using traditional infrared detectors such as InSb or PbS since such measurements require low noise and high-shunt resistance detectors. These measurements are now possible due to the recent development of extended range indium gallium arsenide (exInGaAs) detectors[8]. To increase their shunt resistances and decrease the noise, these detectors are operated with 4-stage thermo-electric cooling to -85 °C and hermetically sealed to avoid condensation. Since the shunt resistances of the exInGaAs detectors are also dependent on the detector area, small, 3 mm diameter detectors are chosen for this work. The shunt resistances of these detectors are between 1 MΩ and 3 MΩ at -70 °C. The noise-equivalent power was 15.4 fW with a 1 s time constant.

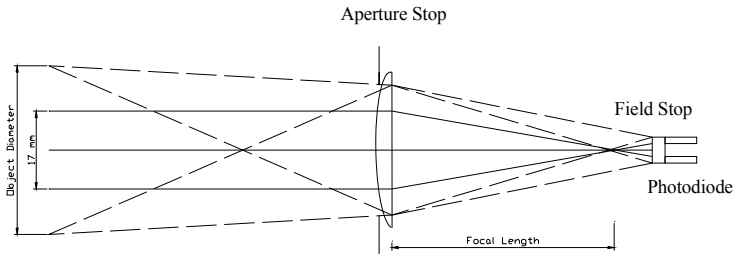

Fig. 4. The radiometer with a simple lens with the schematic of the collection for collimated radiation and diverging radiation. In the collimated geometry, the focus distance is in front of the detector with underfilling of the detector, and in the finite-focus geometry, the active area of the detector defines the collection area.

2.3 Optical Design of the Radiometer

The design of the NIST radiometer was constrained by the fact that it had to be installed adjacent to the Si-based radiometer without affecting the normal operation of the STARR facility in the Si range, and that the radiometer and the imaging optics had to be mounted on the arm of the rotation stage without the total mass of the of radiometer physically altering the geometric alignment of the head. These two constraints limited the optical design of the radiometer, shown in Fig. 4, to the use of a compact 25 mm diameter refractive lens for the wavelength region between 1100 nm to 2500 nm. Although reflective optics would eliminate concerns about chromatic aberrations, the need to measure the incident collimated radiation precluded possible use of Cassegrainian-type collection optics with a central obscuration. Any off-axis mirror geometry would require multiple elements which would exceed the low mass requirement for mounting on the moving stage and might also result in unacceptable image quality in the incident and reflected collection geometries.

For these measurements, a 50 mm focal length bi-convex CaF_2 singlet lens was selected after experimentation with achromats and other multiple element lenses. Since the lens will be utilized over a broad wavelength region, the lens was not anti-reflection coated. Optical elements in the path of the radiation were selected to reduce possible interference fringes as a function of the wavelength. The short focal length lens was chosen to minimize the changes in the image distance with the collimated and reflected geometries. This difference in the image distances arise since in the collimated geometry, the lens operates in an infinite conjugate with the image distance equal to the focal length of the lens. In the reflected geometry, the incident beam reflection from the sample becomes the object and the image distance is changed due to the object being at a finite distance. If the collection lens had a much longer focal length, the larger change in the image distance between the two measurement geometries would result in the image being larger than the 3 mm diameter detector size thus leading to loss of signal in either measurement configuration.

2.4 Sample Translucency Effect

In materials, translucency effects are due to the scattering of the radiation within the material and lateral transport of the radiation. The radiation is then scattered and directed back in the direction of the incident radiation. Any translucency in the reflectance standard will result in a larger radiating area than the spatial extent of the incident radiation due to this migration and subsequent emission. If the optical design of the radiometer is such that the object size is only slightly larger than the incident spot size, then it is possible that the emission from the translucent material will be lost due to migration away from the imaged area[9]. This situation is illustrated in Fig. 4. The radiation in the collimated geometry is focused in front of the detector and the radiation underfills the detector and the objective lens. When the object is at a finite focus distance, the radiation overfills the objective lens and the imaged area is defined by the size of the detector. At NIST, the incident radiation has a beam diameter of 17 mm which is much smaller than the object diameters of either the InGaAs or the Si radiometers at 44.03 mm and 56.05 mm respectively as listed in Table 2. The translucency effect

Table 2. Optical parameters of the Si and InGaAs radiometers.

Detector Type	InGaAs	Silicon
Lens Material	CaF_2	Fused Silica
Focal Length [mm]	50	100
Incident Radiation Diameter [mm]	17	17
Aperture Diameter [mm]	20.3	31.85
Object Distance [mm]	672.6	672.6
Image Distance [mm]	45.83	120
De-Magnification	0.068	0.18
Detector size [mm]	3	10
Object Diameter[mm]	44.03	56.05

will depend on the sample measured as well as the optical arrangement of the radiometer. Due to this large difference in the incident and imaged areas, and since the sintered PTFE sample has been found to exhibit minimal translucency

effects, the translucency effect is not expected to be significant for our measurement geometries. The translucency effect would lead to a net decrease in the reflectance factor in Eq. 1.

2.5 Scatter in the Incident Radiation

Another important systematic correction is the possible scattered radiation (halo) around the incident radiation due to astigmatism within the monochromator[10] and the diffuse forward scatter from contaminants and imperfections on the off-axis parabolic mirror and the flat, folding mirror. The dotted lines on either side of the incident radiation in Fig. 1 illustrate the effect of the scatter. Any scattered radiation around the incident radiation at greater diameters than the aperture stop diameter on the objective lens would be clipped by the aperture stop and not be collected. As seen in Table 2, the object diameter in the measurement geometry for the collection of reflected radiation is much larger than aperture diameter and thus the scattered radiation is collected in the reflected geometry. In the collection of the incident radiation, using the exInGaAs radiometer, the aperture stop diameter of 20.3 mm is just larger than the incident radiation diameter of 17 mm. For the Si radiometer, the aperture stop diameter of 31.85 mm is much larger than the incident radiation diameter of 17 mm. The two radiometers due to the differences in the aperture stops diameters will have different systematic corrections for the scatter in the incident radiation. This scatter will also depend on the cleanliness of the mirrors and could change with time. The scatter is also expected to be dependent on the wavelength since the one would expect greater scatter at shorter wavelengths from the mechanism of scatter from surfaces. This scatter will also change if any optical elements are introduced into the beam path such as depolarizers or polarization rotators.

2.6 Differential Lens Transmittance

A systematic offset between the incident signal and the reflected signals can come from the difference in the area on the objective lens between the measurements of the incident and the reflected signals. As shown in Fig. 4, in the measurement of the incident radiation only the central 17 mm diameter of the lens is utilized, while the entire lens is used in the measurement of the reflected radiation. Since the thickness of the lens changes from the center to the edge, the spectral transmittance of the lens will depend upon the radiated area on the lens due to the change in the thickness and also due to the spatial nonuniformity of the lens transmittance. Large differences in the two measurement setups can be avoided by decreasing the aperture sizes in Table 2 to be just larger than the diameter of the incident radiation. However, this reduction in the aperture size will lead to lower reflected signals and furthermore the rejection of the scatter in the incident radiation will be greater. This effect can also be eliminated by using non-imaging integrating sphere-based radiometers constructed without any lenses, but again the attenuation of the signals due to the sphere throughput and the possible decrease in the signal-to-noise ratio must be balanced against any reduction in the uncertainties.

2.7 Chromatic Focal Shift

The infrared measurements were performed with the 25 mm diameter, bi-convex CaF_2 lens with a nominal focal length of 50 mm. The focal length was chosen to reduce the image size in the reflected geometry with a small de-magnification factor. Since the image spot cannot be directly observed in the infrared wavelengths, the lens was focused at 555 nm and the distance offsets due to chromatic focal shifts calculated using optical modeling software. The image distances will change depending on the object distance and this dependence is listed in Table 3. The image distance in the radiometer was set at 1600 nm focal length with the object at a finite distance as shown also in Fig. 4.

Table 3. Chromatic focal length shifts of the CaF_2 lens. The image distances are determined at 555 nm.

Wavelength [nm]	Object Distance [mm]	Image Distance [mm]
1600	infinite	42.59
555	infinite	41.65
1600	672.6	45.83
555	672.6	44.74

2.8 Polarization Effects

In the measurement setup in STARR, polarization effects arise from the use of the output from monochromator as a quasi-monochromatic source. Although the 100 W QTH lamp source is not polarized, the gratings in the monochromator have polarization-dependent diffraction efficiencies and thus the monochromator output is polarized. If the incident radiation is not randomized with respect to the polarization, then the reflectance measurements can be performed in both the S and P polarizations, and the average value is reported. This doubles the measurement time, and in the infrared region, a depolarizer at the output of the monochromator was selected to scramble the polarization incident on the sample. Initial measurements with the depolarizer indicated that the presence of the thin, parallel separation between the two pieces of the depolarizer led to interference fringes which progressively became larger with increasing wavelength. Since no acceptable solutions to remove the polarization without introducing interference fringes presently exist in STARR, the following measurements were performed without the depolarizer. Since the reflectance properties of Spectralon can have a dependence on the polarization properties of the incident radiation[11], further work is needed to remove the possible polarization dependent reflectance.

3. EXPERIMENTAL RESULTS

The 0°/45° reflectance factors of Spectralon from measurements in STARR and in the ISRF are shown in Fig. 5. The STARR measurements are performed without the depolarizer and also linearly scaled to the measurements in ISRF. The agreement between the two facilities using two different realization paths indicate that the possible effects due to

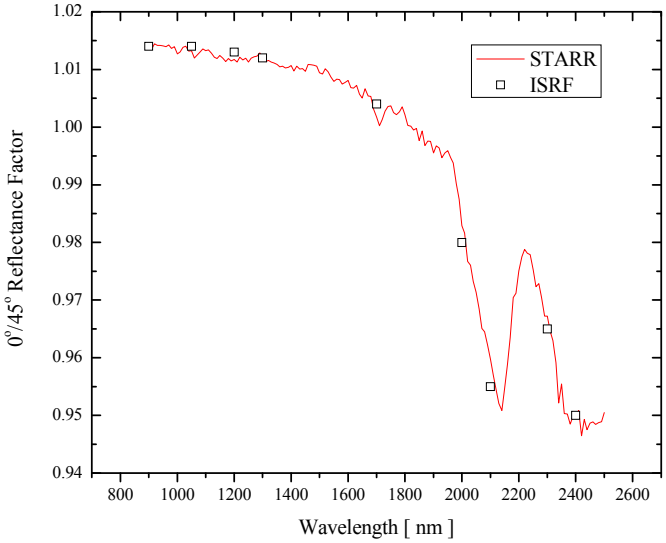

Fig. 5. The 0°/45° reflectance factors of Spectralon from 900 nm to 2500 nm as measured in the ISRF with the measurements from STARR scaled to the ISRF measurements at 900 nm.

polarization in the STARR measurements are minimal. One observes a gradual decrease in the reflectance factor with increasing wavelengths and most importantly the presence of absorption features at 2150 nm and also at 2400 nm. The measurements in STARR were performed at every 10 nm intervals. The measurement wavelengths in the ISRF are limited due to the limited number of calibration wavelengths of the radiance and the irradiance standards. NIST intentionally does not calibrate the standards in wavelength regions where atmospheric absorption can affect the calibrations. Although the radiance and irradiance standards could be interpolated, the presence of OH absorption in the lamp envelopes caused large variations in the interpolated wavelengths and thus the interpolations are not shown.

Until the present work, direct measurement of the 0°/45° reflectance factors beyond 1600 nm could not be performed. For pressed PTFE or Spectralon, a constant ratio between the 6°/h and the 0°/45° reflectance factors were thought to hold beyond 1600 nm from examination of this relationship at shorter wavelengths as shown in Fig. 6. Although the exact ratio could be different, depending on the sample of the Spectralon, a constant ratio between the directional and the hemispherical reflectance factors can be observed from 400 nm to 1600 nm[12,13].

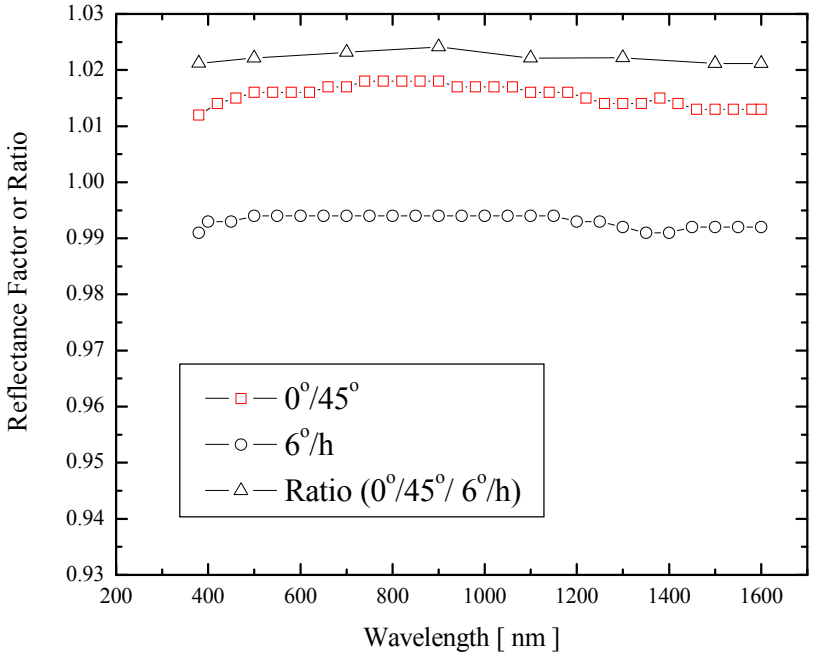

Fig. 6. The 0°/45° and 6°/h reflectance factors of pressed PTFE and their ratios from 400 nm to 1600 nm as measured in STARR from Ref. 12. A constant ratio between the reflectance factors can be observed.

The constant ratio between the reflectance factors in the wavelength region from 400 nm to 1600 nm does not show any wavelength dependence in this region. Although the spectral transmittance of Spectralon does have a wavelength dependence, the presence of a constant ratio with increasing wavelength would indicate that the angular reflectance function has not changed from 400 nm to 1600 nm.

The directional and the hemispherical reflectance factors are plotted for the wavelength region from 900 nm to 2400 nm in Fig. 7. The 0°/45° reflectance factors of Spectralon were measured in ISRF and STARR, and the 6°/h reflectance factors were measured in STARR using its directional-hemispherical integrating sphere. The constant factor between the reflectance factors can be observed to 1600 nm where the 0°/45° reflectance factors start to decrease in the regions of spectral absorption between 2000 nm and 2400 nm. At 2400 nm, the ratio is reduced to 1.008. Thus the assumption of a constant ratio over all wavelengths could lead to a systematic error of about 1.7 % in the wavelength region beyond 1600 nm.

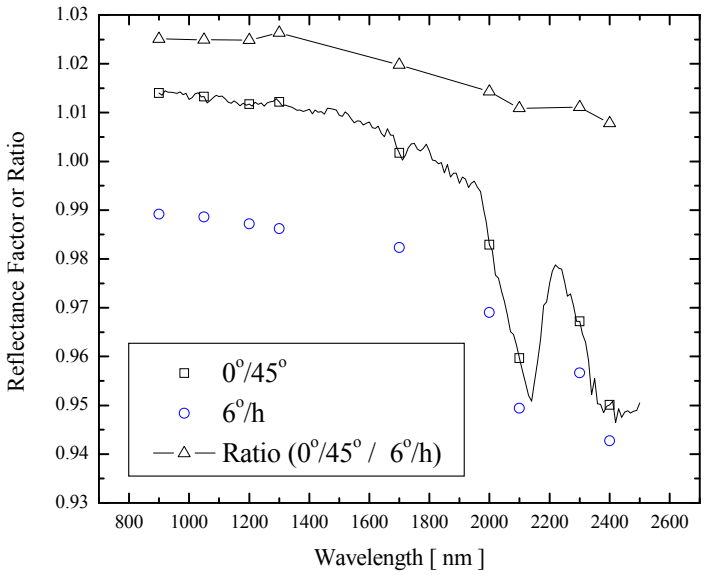

Fig. 7. The 0°/45° reflectance factors and the 6°/h reflectance factors of Spectralon measured in STARR and their ratios from 900 nm to 2500 nm. The constant ratio assumption becomes invalid past 1600 nm possibly due to the chemical absorption seen at 2100 nm and at 2400 nm.

The rapid change in the ratio past 1600 nm is unexpected in light of the constant ratio observed from 400 nm to 1600 nm. However, this change in the angular reflectance function might arise from the presence of strong chemical absorption peaks in Spectralon centered at 2100 nm and at 2400 nm. We speculate that the onset of chemical absorption could lead to a more lambertian reflectance resulting in ratios being close to unity. Further off-angle measurements of the reflectances in this spectral region would be needed to determine if these ideas are correct.

4. DISCUSSION OF UNCERTAINTIES

The estimated uncertainties of the 0°/45° reflectance factors are listed in Table 4. The uncertainties terms can be related to Eq. 1 where the aperture distance and the area are equal to the distance and the aperture area determinations. The viewing angle is the uncertainty related to the setting of the angle in Eq. 1, and the item location is the uncertainty from the movement of the reflectance panel for each measurement wavelength. The detector gain refers to the linearity of the gain determination when the differences between the incident and the reflected signals can be large as listed in Table 1. The determination of gain correction factors is especially important when lock-in detection methods are used since the signal dependence on the chopping frequency must be known. The relatively large wavelength uncertainty of 2 nm is due to the large bandpass of the monochromator of 14 nm used in this wavelength region. The large opening of the monochromator is needed to increase the signal for reduction of the measurement noise. The repeatability of the measurements has been demonstrated to be within the estimated uncertainties. The largest possible source of uncertainty which has not been systematically studied is the issue of polarization dependent reflectance with also a wavelength dependent component.

Table 4. Estimated uncertainties for the 0°/45° reflectance factors in the wavelength region from 900 nm to 2500 nm

Sources of Uncertainty	Standard Uncertainty	Uncertainty Contribution
Aperture Distance	0.3 mm	0.0009
Aperture Area	0.5 mm^2	0.0006
Viewing Angle	0.06º	0.0010
Item Location	0.3 mm	0.0004
Detector Gain	0.06 %	0.0006
Wavelength		
900 nm ≤ λ ≤ 2500 nm	2 nm	0.0010
Illumination Angle	0.1º	0.0010
Viewing Angle	0.1º	0.0002
Uniformity	0.1 %	0.0010
Repeatability		
900 nm ≤ λ ≤ 2500 nm	0.10 %	0.0010
		Expanded Uncertainty (k = 2)
900 nm ≤ λ ≤ 2500 nm		0.0052

5. CONCLUSIONS

We describe the use of an extended-range InGaAs radiometer to determine the $0^o/45^o$ directional reflectance of Spectralon from 900 nm to 2500 nm. The different methods of absolute reflectance measurements are reviewed and the uncertainties in the NIST measurements are listed. These direct reflectance measurements suggest that the ratio between the $0^o/45^o$ reflectance and the 6°/h reflectance factors of pressed PTFE or Spectralon could change in the wavelength region from 1600 nm to 2500 nm possibly due to the presence of chemical absorption features. A full uncertainty budget for the spectral reflectances will be developed with the eventual offering of these measurements as a NIST calibration service.

[#]Certain commercial equipment, instruments, or materials are identified in this paper to foster understanding. Such identification does not imply recommendation or endorsement by the National Institute of Standards and Technology, nor does it imply that the material or equipment are necessarily the best available for the purpose.

REFERENCES

1. J. R. Irons, and J. G. Masek, “Requirements for a Landsat Data Continuity Mission,” Photogrammetric Engineering & Remote Sensing **72**, pp. 1102-1108, (2006).
2. R. A. Barnes and E. F. Zalewski, "Reflectance-Based Calibration of SeaWiFS. II. Conversion to Radiance," Appl. Opt. **42**, 1648-1660 (2003).
3. R. A. Barnes and E. F. Zalewski, "Reflectance-Based Calibration of SeaWiFS. I. Calibration Coefficients," Appl. Opt. **42**, 1629-1647 (2003).
4. D.Hunerhoff, U.Gruseman, A.Hope, “New robot-based gonioreflectometer for measuring spectral diffuse reflection“, Metrologia **43**, S11-S16, (2006).
5. S. Nevas, F. Manoocheri, and E. Ikonen, “Gonioreflectometer for measuring spectral diffuse reflectance”, Applied Optics **43**, 6391-6399 (2004).
6. P. Y. Barnes, E. A. Early, and A. C. Parr, “NIST Measurement Services: Spectral Reflectance”, NIST Special Publication 250-48, 1998.
7. W. R. McCluney, *Introduction to Radiometry and Photometry*, Artech House, Boston, 1994.
8. H. W. Yoon, M. C. Dopkiss, G. P. Eppeldauer, “Performance Comparisons of InGaAs, extended InGaAs, and Short-wave HgCdTe Detectors between 1 μm and 2.5 μm”, Infrared Spaceborne Remote Sensing XIV, Proc. of SPIE Vol. **6297**, 629703, (2006).

9. S. Holopainen, F. Manoocheri, E. Ikonen, K. Hauer, and A. Höpe, “Comparison measurements of 0°/45° radiance factor and goniometrically determined diffuse reflectance”, Applied Optics **48**, pp.2946-2956 (2009).
10. S. Holopainen, F. Manoocheri, S. Nevas, and E. Ikonen, “Effect of light scattering from source optics in goniometric diffuse reflectance measurements”, *Metrologia* **44**, 167-170 (2007).
11. G. T. Georgiev and J. J. Butler, “The Effect of incident light polarization on Spectralon BRDF measurements”, Sensors, Systems, and Next-Generation Satellites VIII, Proceedings of SPIE Vol. **5570**. pp. 492-502. (2004).
12. M. E. Nadal and P. Y. Barnes, “Near infrared 45°/0° reflectance factor of pressed polytetrafluoroethylene (PTFE) powder”, J. Res. Natl. Inst. Stand. Technol. **104**, 185-188(1999).
13. D. C. Williams, “Establishment of absolute diffuse reflectance scales using the NPL Reference Reflectometer,”, Analytica Chimica Acta **380**, 165-172, (1999).